Fluid Dynamic Effects of Grooves on Circular Cylinder Surface

Takeyoshi Kimura* and Michihisa Tsutahara†
Kobe University, Kobe 657, Japan

It is shown that a groove on the surface of a circular cylinder affects movement of the separation point backward and reduces drag even at Reynolds numbers of about a few thousand. Several types of circular-arc cross-section grooves are studied using flow visualizations and numerical simulations. Whether these grooves are effective depends strongly on their positions, and the most effective positions are about 80 deg, measured from the foremost point. When they are effective, cavity flows are developed inside the grooves. This effect corresponds to that of dimples on golf balls and will explain unique characteristics of the drag curve.

Introduction

IN this study, a circular-arc groove on the surface of a circular cylinder will be shown to have an effect on reducing drag on the cylinder, and the effect is considered similar to that of dimples of golf balls.

It is widely known that dimples of a golf ball reduce dramatically the aerodynamic drag of the ball. The reason is also widely explained as the effect of roughness on the surface of the sphere; i.e., it changes the laminar boundary layer to the turbulent boundary layer, and the separation point moves backward.

A careful measurement, however, of the drag on the golf ball by Bearman and Harvey[1] shows that the drag curve of a golf ball against the Reynolds number is different from that of spheres with surface roughness,[2] as shown in Fig. 1. The drag coefficients drop at the critical Reynolds number. However, as the Reynolds number increases, the drag coefficients of the spheres with roughness increase again. Conversely, the drag coefficient of the golf ball remains almost constant. This implies that the dimples have another effect on the drag reduction of the golf balls, in addition to promoting boundary-layer transition.

The difference between the dimples and the roughness is apparently the sizes of the two. The dimples have spherical shape and are much larger than ordinary roughness scales. Therefore, it is natural to consider that some cavity flow exists inside the dimples. We expect that this cavity flow is the reason the drag curve behaves uniquely; i.e., the drag coefficient remains almost constant. The roughness thickens the turbulent boundary layer and the separation occurs earlier, and then the drag coefficient rises. However, the dimples will not alter the flow pattern by the cavity flows inside them over a wide range of the Reynolds number, from 6×10^4 to 3×10^5 (Bearman and Harvey[1] obtained data up to this value, but the drag coefficient is expected to remain almost constant at higher Reynolds numbers).

Moreover, these cavity flows cause the separation point to move backward. This will be explained by a two-dimensional groove instead of three-dimensional dimples as follows. Here we define the edge of the groove on the upstream side as the leading edge and the other as the trailing edge. As shown in Fig. 2, if there is a cavity flow, then the boundary layer separates at the leading edge and reattaches at the trailing edge, or at some other point inside the groove. Although the boundary layer flows over the cavity without touching the cylinder surface, it does not suffer the strong shearing stress from the surface and flow velocity decreases only slightly. This results in a new type of boundary-layer control and causes the separation point to move backward.

If the cavity flows have the aforementioned effect, they are effective for either the laminar or turbulent boundary layer. When the boundary layer is turbulent, the two effects—turbulent separation and cavity flows—are difficult to separate.

Therefore, in this paper, the experiments and numerical simulations were performed at a Reynolds number of about a few thousand, at which the boundary layers remain laminar. The two-dimensional circular cylinder and circular groove were used for convenience of flow visualization and numerical simulation. The differences between the two- and three-dimensional flows corresponding to the flows about golf balls are discussed.

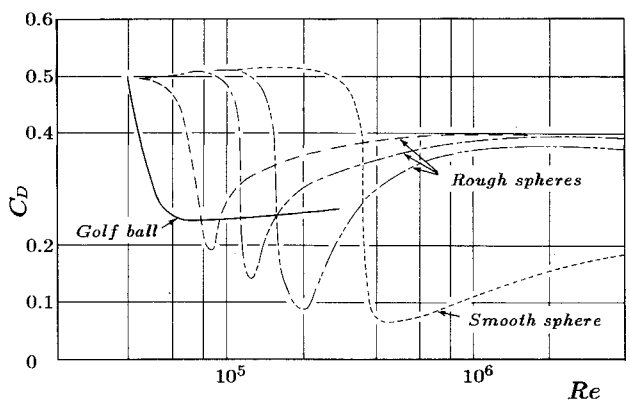

Fig. 1 Curves of drag coefficients for a golf ball and rough surface spheres; reproduced from Ref. 1.

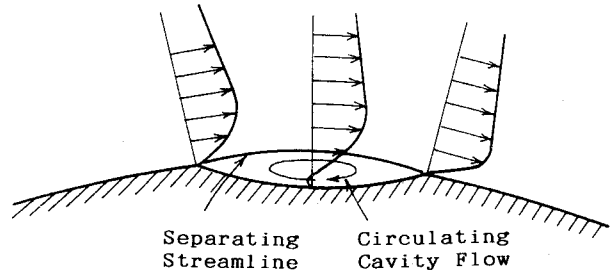

Fig. 2 Cavity flow in the groove.

Received April 27, 1990; revision received Oct. 17, 1990; accepted for publication Nov. 5, 1990.

*Professor, Department of Mechanical Engineering, Rokko, Nada-ku. Member AIAA.

†Associate Professor, Department of Mechanical Engineering, Rokko, Nada-ku. Member AIAA.

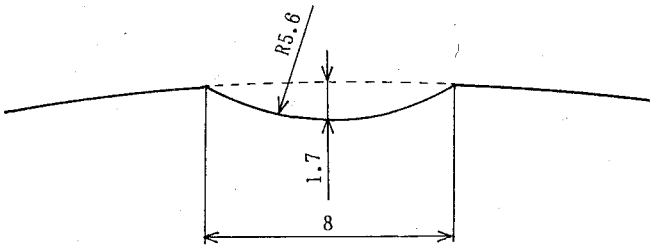

a) Type 1

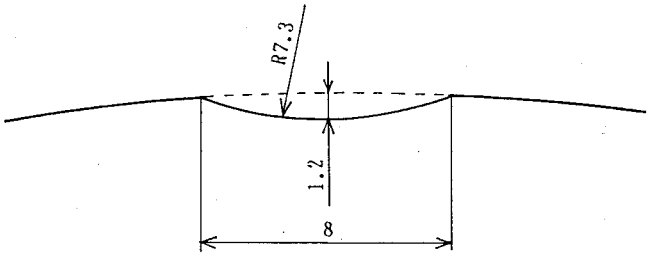

b) Type 2

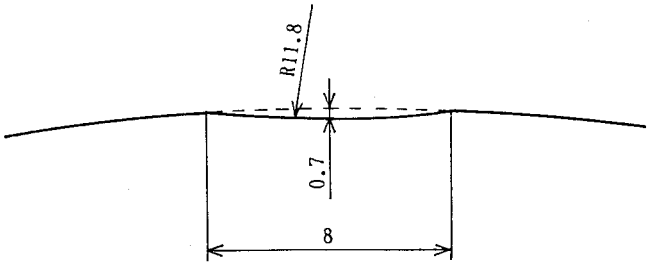

c) Type 3

Fig. 3 Circular-arc grooves.

Flow Visualization

Flow visualization was performed using a circulating water tank, which consists of a 2600 × 500-mm open channel and a tank, both upstream and downstream of the channel. The intensity of turbulence of the flow was about 2%. All of the experiments for the visualization were done at a flow velocity of 2.5 cm/s, which corresponds to a Reynolds number of 2200 based on the cylinder diameter. Also note that, for all of the cases, the boundary layers downstream of the groove were confirmed to remain laminar by measuring the velocity fluctuations with hot-wire probe.

Three types of grooves shown in Fig. 3 were studied and a smooth circular cylinder without grooves was also used for comparison. All of the chord lengths of the grooves were 8 mm, and the groove mentioned by type 2 corresponded to the geometry of the dimples used widely. Type 1 was slightly deeper, and type 3 was slightly shallower.

The cylinders were made of nylon, 100 mm in diameter and175 mm in length. The clinder aspect ratio was not large enough, and the blockage ratio was nonnegligible. However, for estimating the effect of the grooves qualitatively or relatively, these models were sufficient because all of the measurements were done under the same conditions.

There was a free surface in the channel, and the upper side of the cylinder was just at the level of the free surface. There were no visible waves on the surface while the experiments were being carried out. A 3-mm-thick thin plate of 300 mm in diameter was attached to the lower side of the cylinder, and a 4-mm space was opened between the bottom of the channel and the plate to avoid the boundary layer developing on the bottom surface of the channel.

The positions of the groove and the separation point are represented by an angle θ measured from the foremost point of the cylinder, as usual. On the cylinder surface, only one groove is located on one side of the cylinder, so that the geometry is asymmetric with respect to the flow direction.

Timelines about the grooves obtained using the hydrogen bubble method for $\theta = 80$ deg are presented in Fig. 4. It is seen that a separating streamline detached at the trailing edge and reattached at the surface in the groove forms a closed circulating cavity flow for types 1 and 2. However, there is no such circulating flow for type 3.

Some streaklines obtained using the dye injection method are presented in Fig. 5 for type 1. A red ink thinned with water

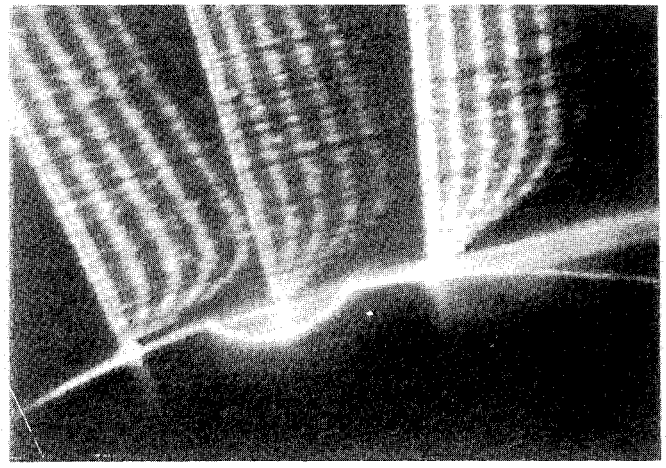

a) Type 1

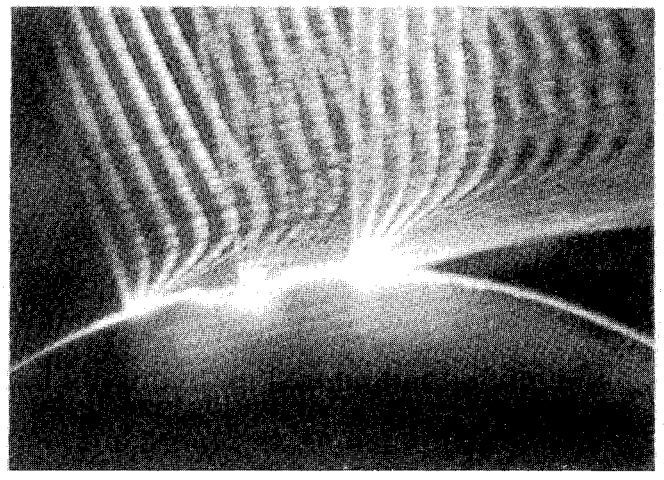

b) Type 2

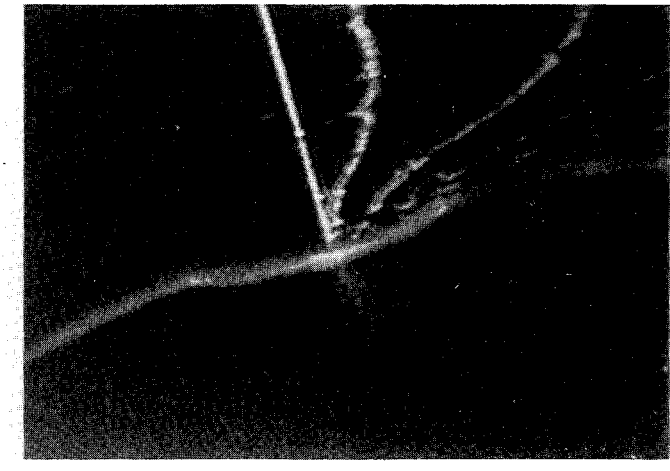

c) Type 3

Fig. 4 Timelines about the grooves.

Table 1 Positions of grooves and separation points (deg) (At 90 deg, separation occurs at groove leading edge)

Type θ	50	60	70	75	80	83	85	90
Smooth				92.0				
Type 1	92.0	91.0	93.0	93.0	94.0	94.5	94.0	85.5
Type 2	91.5	91.5	92.5	93.0	94.0	94.5	93.5	85.5
Type 3	92.0	91.5	92.0	92.5	92.5	94.0	93.0	85.5

was used for the tracer, and it was injected through a thin injector's needle. Once the dye was injected, the needle was removed so as not to disturb the flow. The separation points are also seen clearly using the streaklines.

The separation points and the positions of the groove are presented in Table 1. The separation points changed their positions 4 or 5 deg during the experiment corresponding to the periodic wake flow. The separation points presented in the table are their average values. The resolution of the determination of the separation point was about 0.5 deg; therefore, the angles in the table are shown at 0.5-deg intervals.

The grooves have no effect when the position is less than 75 deg. Among these grooves, the most effective is type 2 at $\theta = 83$ deg.

The flows about the grooves when they are at the most effective positions (83 deg) are sketched and shown in Fig. 6.

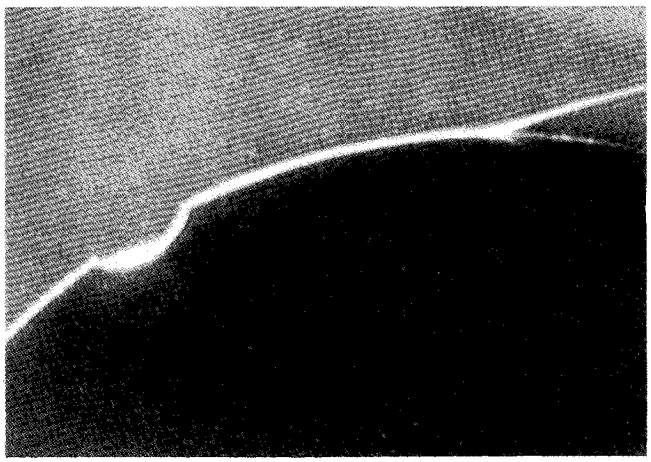

a) $\theta = 60°$

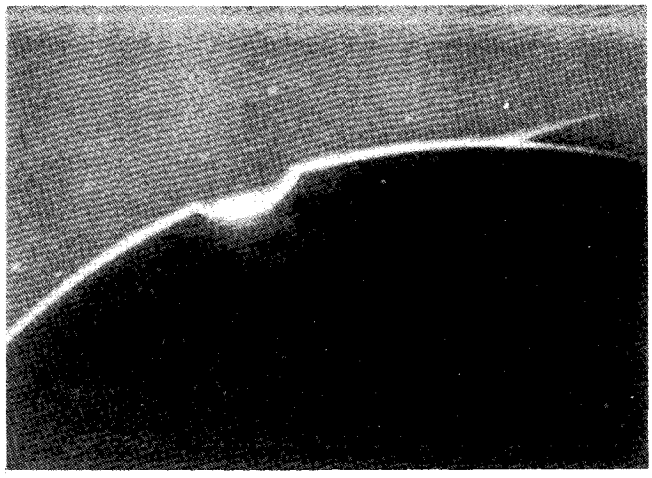

b) $\theta = 70°$

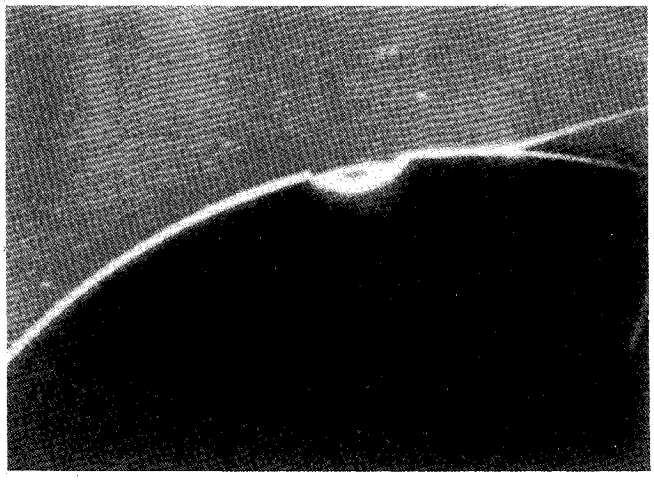

c) $\theta = 80°$

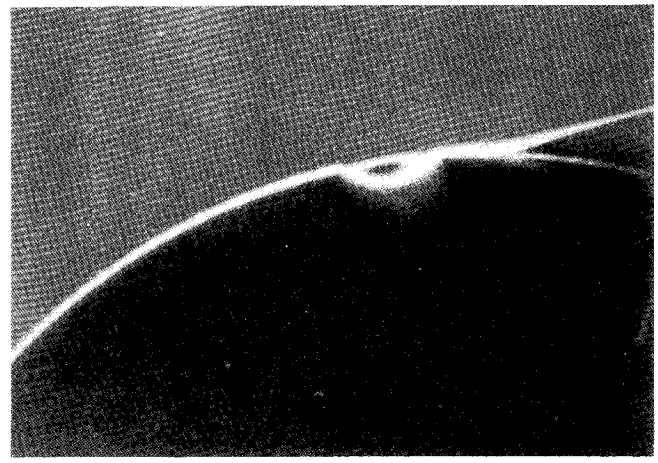

d) $\theta = 83°$

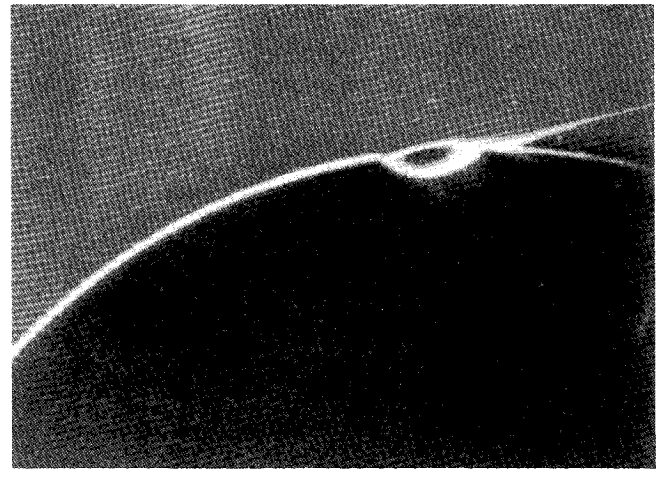

e) $\theta = 85°$

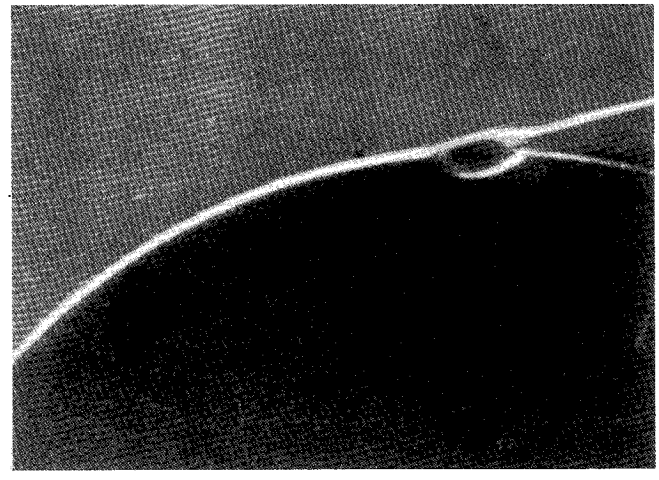

f) $\theta = 90°$

Fig. 5 Streaklines about type 1 groove.

Closed circulating flows exist over almost the whole area of the grooves for types 1 and 2. Although there is no circulating flow for type 3, this groove is also effective, and the reason is considered later.

Numerical Simulations

To confirm the effect of the groove on moving the separation points backward and to obtain more detailed information of the flow, the two-dimensional Navier-Stokes equations were calculated numerically using the finite difference method. Three flows were chosen, i.e., the flows about the smooth cylinder and those about two types of cylinders; one of which has the groove of type 2 presented in Fig. 3, and the other has a much shallower groove with a depth of 1% of the cylinder's diameter (the groove is represented as type 4). The position of the groove was chosen at 80 deg for both grooves, and on each cylinder there are two grooves at the symmetric positions with respect to the flow direction.

The mesh was constructed using the boundary-fitted coordinates introduced by Thompson and Thames.[4] The physical plane (x,y) is transformed into the calculation plane (ξ,η) by

$$\alpha x_{\xi\xi} - \beta x_{\xi\eta} + \gamma x_{\eta\eta} + J^2(Px_\xi + Qx_\eta) = 0 \tag{1a}$$

$$\alpha y_{\xi\xi} - \beta y_{\xi\eta} + \gamma y_{\eta\eta} + J^2(Py_\xi + Qy_\eta) = 0 \tag{1b}$$

where

$$J = x_\xi y_\eta - x_\eta y_\xi \tag{2a}$$

$$\alpha = x_\eta^2 + y_\eta^2 \tag{2b}$$

$$\beta = x_\xi x_\eta + y_\xi y_\eta \tag{2c}$$

$$\gamma = x_\xi^2 + y_\xi^2 \tag{2d}$$

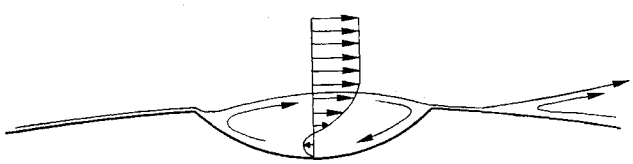

a) Type 1

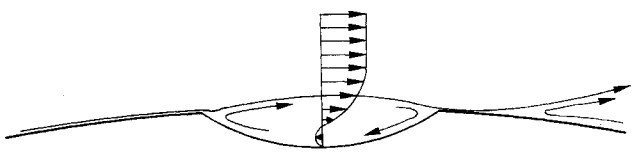

b) Type 2

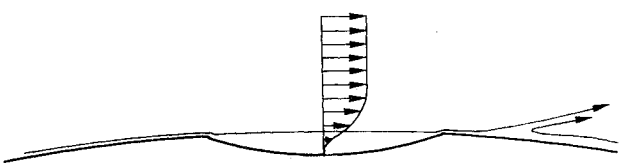

c) Type 3

Fig. 6 Sketch of flows in grooves when most effective.

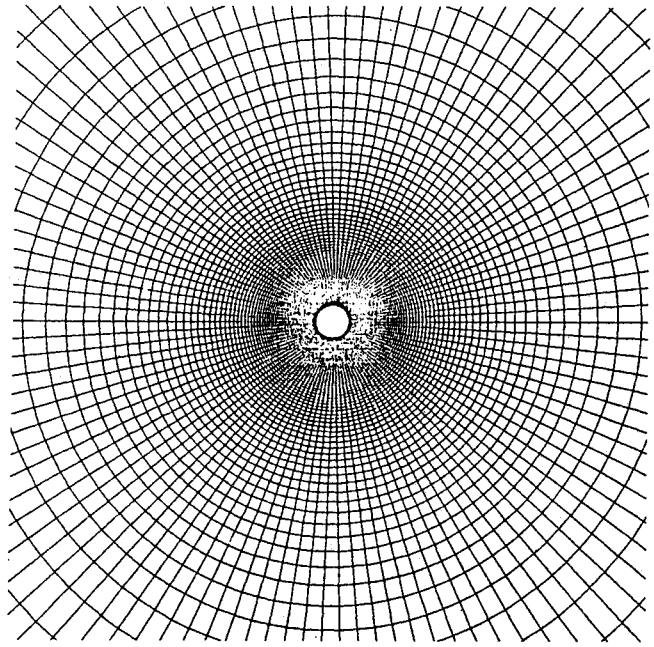

a)

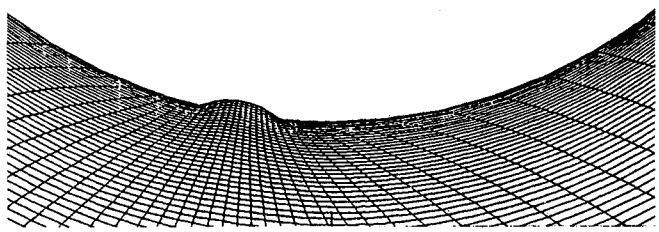

b)

Fig. 7 Grid for grooved cylinder.

Equations (1) are solved numerically with the boundary condition

$$x = f_1(\xi,\eta_0), \qquad y = f_2(\xi,\eta_0)$$

$$x = g_1(\xi,\eta_\infty), \qquad y = g_2(\xi,\eta_\infty) \tag{3}$$

where the subscript 0 refers to the value on the surface and ∞ is infinity. The parameters P and Q are introduced to control the density of the mesh and were chosen as

$$P = 0$$

$$Q = -4000\exp[-0.1(\eta-\eta_0)] \tag{4}$$

A closed curve $\eta = \text{const}$ was taken on the surface of the cylinder, including the bottoms of the grooves, and the number of the grid points were 111×121. The outer boundary was taken on a circle with a radius 30 times larger than the cylinder's. As shown in Fig. 7, the mesh was made dense near the groove, and about 10 grid points were inserted in the η direction within the boundary layer.

The Navier-Stokes equations are nondimensionalized and formulated using the streamfunction ψ and the vorticity ω as

$$\omega_t + (1/J)(\psi_\eta\omega_\xi - \psi_\xi\omega_\eta)$$

$$= (1/ReJ^2)(\alpha\omega_{\xi\xi} - 2\beta_{\xi\eta} + \gamma\omega_{\eta\eta}) + (1/Re)(Q\omega_\eta + p\omega_\xi) \tag{5}$$

$$(1/J^2)(\alpha\psi_{\xi\xi} - 2\beta\psi_{\xi\eta} + \gamma\psi_{\eta\eta}) + Q\psi_\eta + P\psi_\xi = -\omega \tag{6}$$

The boundary conditions on the cylinder surface are

$$\psi_0 = 0 \tag{7}$$

$$\omega_0 = -(\gamma/J)\psi_{0\eta\eta} \tag{8}$$

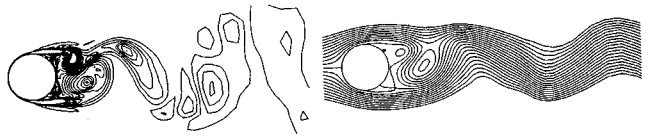

a) Smooth

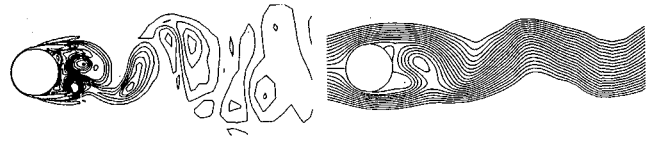

b) Type 2

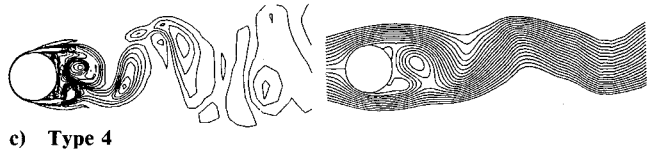

c) Type 4

Fig. 8 Equivorticity lines and streamlines at nondimensional time 20. Note that the distance between two successive vertices is smaller for the grooved cylinder than for the smooth cylinder.

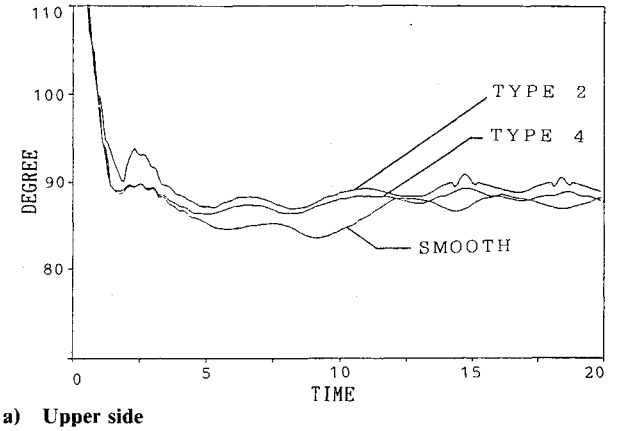

a) Upper side

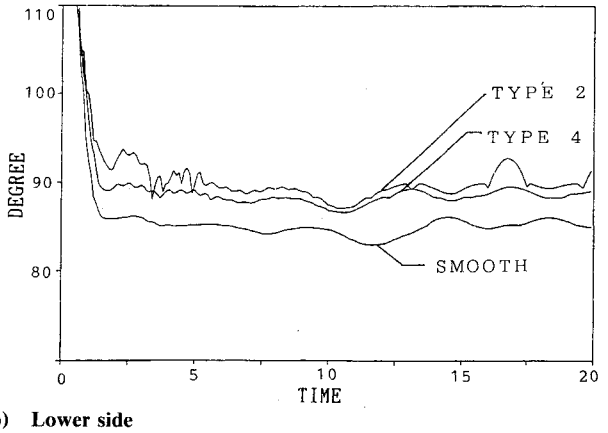

b) Lower side

Fig. 9 Time histories of separation points on upper and lower sides.

Equation (8) represents the no-slip condition. The conditions at the outer boundary are the freestream as

$$\psi_\infty = y_\infty, \qquad \omega_\infty = 0 \tag{9}$$

The integration of Eqs. (5) and (6) was done using Euler's explicit method and the successive over-relaxation (SOR) method, respectively. For discretizing Eqs. (5) and (6), central differences of the second order

$$\frac{\partial f}{\partial \xi_{i,j}} = \frac{f_{i+1,j} - f_{i-1,j}}{2h} \tag{10}$$

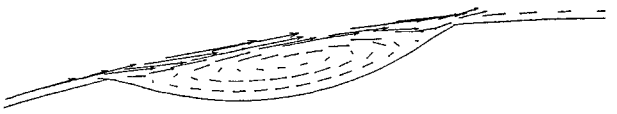

a) Type 2

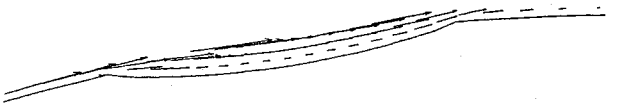

b) Type 4

Fig. 10 Velocity fields about grooves.

$$\frac{\partial^2 f}{\partial \xi_{i,j}^2} = \frac{f_{i+1,j} - 2f_{i,j} + f_{i-1,j}}{h^2} \tag{11}$$

were employed except for the nonlinear convection term in Eq. (5). For that term, the third-order Kawamura's scheme[5]

$$\left(g\frac{\partial f}{\partial \xi}\right)_{i,j} = g_{i,j}\frac{-f_{i+2,j} + 8(f_{i+1,j} - f_{i-1}) + f_{i-1,j}}{12h} + \frac{-4f_{i+1,j} + 6f_{i,j} - 4f_{i-1} + f_{i-1,j}}{4h} \tag{12}$$

was used in discretizing the differentiations with respect to ξ, i.e., the direction of circumference. In Eqs. (10–12), g and f are arbitrary functions of ξ and η, and they are not identical to those in Eqs. (3).

A flow Reynolds number of 1200 was chosen because low-Reynolds-number flows are easier to calculate, and the drag coefficient is almost the same[6] for Reynolds numbers from 1000 to 2500, so that the correspondence between experiment and numerical calculation is acceptable. Of course, the details of the flows will differ, but in this paper the effect of the groove is proved rather independently by experiments and numerical simulations; therefore, the Reynolds numbers in both are not necessarily the same.

Equivorticity lines and streamlines for the three cylinders are presented in Fig. 8. The Strouhal numbers of the wake are about 0.25 for the smooth cylinder, 0.28 for type 2, and 0.27 for type 4. Roshko[3] has reported that the reverse number of the Strouhal number and drag coefficient have a strong relationship, so that the Strouhal numbers mentioned earlier refer to the decreases of the drag coefficient for the grooved cylinders.

The separation points are defined as points where the vorticity on the surface becomes zero, and time histories of the points are shown in Fig. 9. On the upper and lower sides, the separation points for grooved cylinder are retreated by 3–7 deg compared with those for the smooth cylinder.

The velocity fields about the grooves are shown in Fig. 10, in which a closed circulating flow exists for type 2 but not for type 4. The velocity distributions in the boundary layers for the three cylinders are shown in Fig. 11. This shows that the velocities near the bottoms of the boundary layers downstream of the grooves are larger than at the same point for the smooth cylinder. The larger velocities correspond to the retreat of the separation points. It is noted here that type 4 is effective although it has no closed circulating flow, which corresponds to type 3 in the experiments.

The vorticity distributions about the grooves are shown in Fig. 12, where the vorticity at the corresponding occurrence of the smooth cylinder is also shown for comparison. This figure shows the equivorticity lines, then the reason for the aforementioned facts can be explained as follows. The vortices in the grooves, even in the shallow groove without the circulating flow, are smaller than on the surface of the smooth cylinder,

which leads to smaller shearing stresses. Therefore, these grooves are effective even if there are no circulating flows.

The preceding facts are a reminder of the laminar separation bubbles at the critical Reynolds number, whose effect on the reduction of the drag may be the same as that of a very shallow groove, although one is concave and the other is convex.

It will be apparent that the shearing stress on the cylinder's surface increases when the grooves are effective and the drag due to the friction increases. However, the increase of friction will be much smaller than the decrease of drag due to the pressure.

The pressure distributions and the drags on the cylinder were not obtained in the present simulation. The reason is that the pressure is not single-valued around the cylinder's surface when Eq. (7) is employed for the boundary condition there, although this condition is often used for this type of problem. To make the pressure single-valued, the value of the streamfunction on the surface must be changed and suitably chosen.[6] However, the calculation for converging this value was very time-consuming. Then symmetricity of the upstream flow was assumed and the error of the pressure was neglected in this simulation. However, the jump of the pressure is within several percent of the maximum value of $p_s - p_\infty$, where p_s and p_∞ are pressure on the surface and at infinity, respectively. Therefore, the error in the flowfield at each point is very small, and the separation points would be almost unchanged even when the error was reduced. Conversely, the differences in the drag among the cases presented herein are essentially very small, so that the error is significant for comparing the drags, and the calculation of the drag does not have physical meaning. Then only the comparison of the separation points was done, not the drag.

Discussion

The effect of a golf ball's dimples was studied in a two-dimensional model. Of course, there are many differences between the two- and three-dimensional flows. For example, in the two-dimensional flow, inside the groove a closed circulating cavity flow can exist stably; in three-dimensional dimples, the circulation cannot close inside the dimples, and the vorticity lines will go outside as horseshoe vortices. These horseshoe vortices are the main cause for the transition of the laminar boundary layer to a turbulent boundary layer.

The results obtained in two-dimensional flow, however, will hold qualitatively even in three-dimensional flows. Moreover, the results presented herein will be useful for reducing the drag on two-dimensional blunt cylinders, such as tall chimneys or bridge girders.

The flow Reynolds number in this study was a few thousand and the boundary layer was kept laminar. However, the effects of the dimples or the grooves, as a result of cavity flows inside them, will create higher Reynolds number flows in which the boundary layer ahead of the dimples or grooves is turbulent, because the cavity flow will apparently be formed in such flows.

Therefore, they will still be effective at the so-called transcritical Reynolds numbers, which are much higher than the critical ones. Actually, the structures presented here suffer huge aerodynamic force at this Reynolds number region, and drag reduction at this region is very effective in reducing costs.

The effect of the grooves depends on their position. At about 80 deg, they are most effective. In the experiment in this study, the Reynolds number is small, so that the grooves have almost no effect when their positions are less than 70 deg. However, when the Reynolds number is much higher, the grooves will have negative effects if they are in small angles because the separating streamline from the leading edge must clash in the bottom of the groove. This will significantly de-

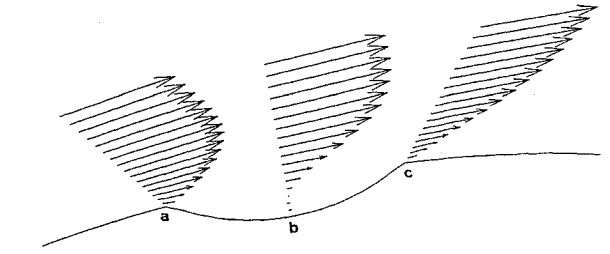

a) Type 2

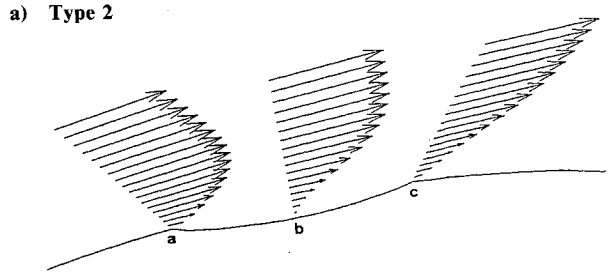

b) Type 4

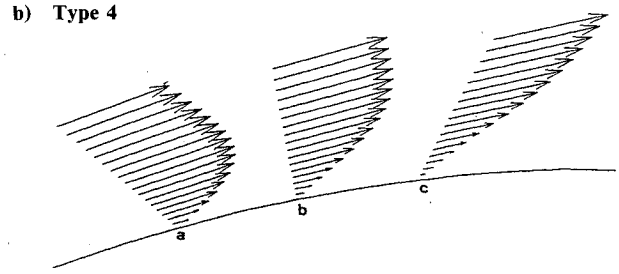

c) Smooth

Fig. 11 Velocity distributions in boundary layers.

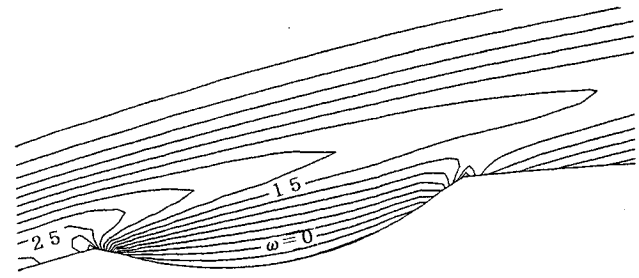

a) Type 2

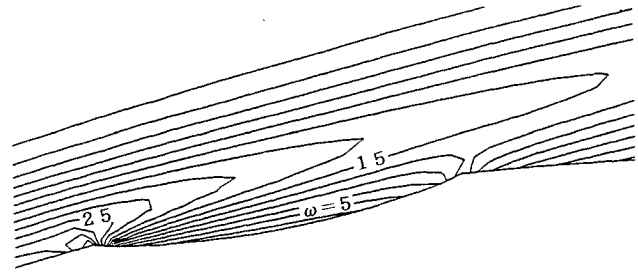

b) Type 4

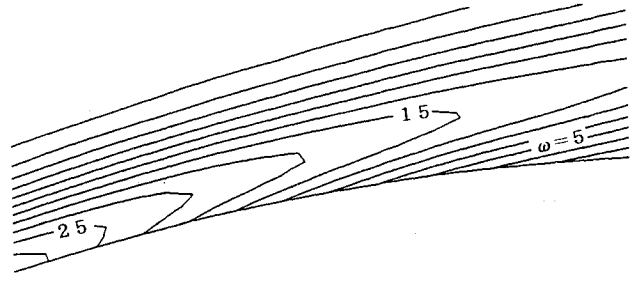

c) Smooth

Fig. 12 Vorticity fields about grooves.

crease the velocity of the boundary layer. The drag coefficient of the golf balls at the critical Reynolds number is not that small compared with other spheres with roughness, as shown in Fig. 1. This is because the effect of the dimples at good positions is canceled by the negative effect by those in the front face of the balls.

So far, the effect of the cavity flow inside the dimples or grooves has been considered. However, it must be remembered that when golf balls are traveling at ordinary speed, the most important effect of the dimples on drag reduction is the same as roughness, i.e., changing the boundary layer to turbulence. It must be emphasized that the dimples or grooves having large enough scale have effects other than roughness.

The separation points for the smooth cylinder—92 deg in the experiments and 87 deg in the numerical calculations—are larger than 80–85 deg of the laminar separation. In the experiments, the blockage ratio is 0.2 and the effect of the sidewalls will cause the large value of the separation point. Considering this effect, it might be modified to a value similar to that in the numerical simulations. However, they still seem large. According to Goldstein,[7] however, the abovementioned laminar separation points are those at Reynolds numbers of about 10^4, at which the drag coefficient is about 1.2, although the drag coefficient is slightly lower and is about 0.9 at Reynolds numbers of about 2000. Although the authors have no data on the separation points at Reynolds numbers of about 2000, they should be slightly larger than the ordinary laminar separation points. Therefore, the values obtained in this study are reasonable.

In this study, no drag on the circular cylinder was obtained directly either in the experiments or by numerical simulation. However, the grooves were effective moving the separation points backward; therefore, they must be effective reducing the drag.

Conclusions

Cavity flows in a groove on a circular cylinder surface are shown to be effective in moving the laminar separation point backward by flow visualizations and numerical simulations. Conclusions obtained are as follows.

1) The grooves are most effective when they are at about 80 deg.

2) When they are most effective, there is closed circulating flow over the cavity.

3) In shallow grooves there is no circulating flow detected, but they are also effective.

4) The effect of dimples on golf balls is considered to be the same as that of the grooves.

Acknowledgments

The authors are indebted to P.W. Bearman of Imperial College for his valuable comments. They are also grateful to K. Kamata and Y. Ikushima for their help in this study.

References

[1]Bearman, P. W., and Harvey, J. K., "Golf Ball Aerodynamics," *Aeronautical Quarterly,* May 1976, pp. 112–122.

[2]Ackenbach, E., "The Effects of Surface Roughness and Tunnel Blockage on the Flow Past Spheres," *Journal of Fluid Mechanics,* Vol. 65, Pt. 1, 1974, pp. 113–125.

[3]Roshko, A., "Experiments on the Flow Past a Circular Cylinder at Very High Reynolds Number," *Journal of Fluid Mechanics,* Vol. 10, Pt. 1, 1961, pp. 245–273.

[4]Thompson, J. F., and Thames, C., "Numerical Solution for Viscous and Potential Flow about Arbitrary Two-Dimensional Bodies Using Body-Fitted Coordinate Systems," *Journal of Computational Physics,* Vol. 24, No. 1, 1977, pp. 245–273.

[5]Kawamura, T., "Direct Simulation of Flows at High Reynolds Number Using a Third-Order Upwind Scheme," *Recent Studies on Turbulent Phenomena,* edited by T. Tatsumi, Association for Science Documents Information, Tokyo, 1985, pp. 117–130.

[6]Matida, Y., Kuwahara, K., and Takami, H., "Numerical Study of Steady Two-Dimensional Flow Past a Square Cylinder in a Channel," *Journal of the Physical Society of Japan,* Vol. 38, No. 5, 1975, pp. 1522–1529.

[7]Goldstein, S. (ed.), *Modern Developments in Fluid Dynamics,* Vol. 2, Dover, New York, 1965, pp. 418–424.